Performance Analysis of UAV Relay NOMA-MEC in IoT Network: Offloading and Optimization

Anh-Nhat Nguyen
ICT Department
FPT University
Hanoi 10000, Vietnam
nhatna3@fe.edu.vn

Gia-Huy Nguyen
ICT Department
FPT University
Hanoi 10000, Vietnam
huynghe180064@fpt.edu.vn

Khai Nguyen
ICT Department
FPT University
Hanoi 10000, Vietnam
khainhe176049@fpt.edu.vn

Minh-Sang Nguyen
ICT Department
FPT University
Hanoi 10000, Vietnam
sangnmhe176048@fpt.edu.vn

Tung-Son Ngo
ICT Department
FPT University
Hanoi 10000, Vietnam
sonnt69@fe.edu.vn

Manh-Duc Hoang
ICT Department
FPT University
Hanoi 10000, Vietnam
duchm29@fe.edu.vn

Tien-Dat Trinh
ICT Department
FPT University
Hanoi 10000, Vietnam
dattt67@fe.edu.vn

Tuan-Anh Hoang
ICT Department
FPT University
Hanoi 10000, Vietnam
anhht68@fe.edu.vn

***Abstract*—This paper investigates unmanned aerial vehicle (UAV) and nonorthogonal multiple access (NOMA)-mobile-edge computing (MEC) in the Internet of Things (IoT) network, where a UAV acts as a relay. To evaluate offloading performance, we derived closed-form formulas for the successful computation probability (SCP) using the Nakagami-m fading channel model. Furthermore, we also propose an optimization problem to maximize SCP by optimizing the UAV deployment location using the genetic algorithm (GA) method. Finally, numerical results are presented to demonstrate the validity of our analysis.**

***Index Terms*—unmanned aerial vehicle, nonorthogonal multiple access, mobile-edge computing, Internet of Things**

I. Introduction

Mobile data traffic in Internet of Things (IoT) has grown rapidly, posing a challenge for mobile devices with limited energy and computing power to handle demanding applications like virtual reality and autonomous driving [1]. To address this, researchers suggest using mobile-edge computing (MEC) and nonorthogonal multiple access (NOMA) for IoT networks [2], [3]. MEC allows mobile devices to use nearby computational resources [4], while NOMA lets multiple devices share the same time/frequency resources through power domain techniques [5]. The combination of NOMA and MEC has recently improved offloading efficiency [6]–[8]. For example, Lin *et al.* investigated the effect of NOMA on computation offloading decisions in MEC systems. Initially, the computation offloading probability is derived using stochastic geometry and order statistics, offering valuable guidelines for deploying NOMA-based MEC systems [6]. Dong *et al.* examined the offloading performance of cooperative NOMA-based MEC, providing detailed exact expressions for the offloading outage probability (FOP) for tasks of two users [7]. Jiang *et al.* examined the offloading performance of uplink NOMA-based MEC with both imperfect and perfect channel state information (CSI). Detailed exact and asymptotic expressions for the FOP of paired users were derived [8].

The success of MEC depends heavily on the data and computing interactions between edge devices (EDs) and servers. Random positioning of EDs can lower signal reception efficiency, and the limited power of EDs restricts their transmission range [9]. Using UAVs for wireless communication can address these issues [10]. UAVs provide Line-of-Sight (LoS) linkages with EDs, which reduce small-scale fading, enhance network performance, and offer reliable signal coverage [11]. UAVs can approach EDs closely, ensuring reliable communication, and acting as airborne edge servers [12]–[14]. For example, A. Umar *et al.* introduced a novel uplink NOMA-based MEC-enabled aerial-vehicular network operating at mmWave frequencies, aimed at minimizing overall computation and communication overhead [12]. G. Huy *et al.* examined a UAV-assisted NOMA-based MEC system, focusing on two resource-limited IoT device clusters and a UAV equipped with a MEC server that also serves as a wireless power transfer station [13]. X. Meng *et al.* investigated a NOMA-based MEC network with UAV. The primary focus is on investigating computation capacity in terms of throughput, defined by the total size of completed tasks through air-ground collaboration [14].

This study investigates offloading efficiency in IoT networks using UAV relay-assisted NOMA-based MEC over Nakagami-m fading channels, considering both LoS and non-LoS (NLoS) scenarios in UAV-EDs communication. An optimization problem is proposed to enhance offloading performance. The primary contributions of the paper are:

- We investigate the best ED and best antenna selection scheme for UAV relay-assisted task offloading in IoT networks over Nakagami-m fading channels. A system protocol is proposed for effective offloading.
- Closed-form expressions for SCP across the entire system are derived. Additionally, we tackle the challenge of optimizing UAV deployment positions to maximize SCP

using a GA algorithm.

- Numerical results validate system effectiveness, including average transmission power, number of EDs per cluster, number of base station (BS) antennas, and UAV position and altitude.

The rest of this paper is structured as follows: Section II introduces the system model and communication protocol. Section III analyzes the SCP and the optimization problem. Section IV presents and discusses the numerical results. Finally, the conclusions are drawn in Section V.

II. Network Model

A. System model

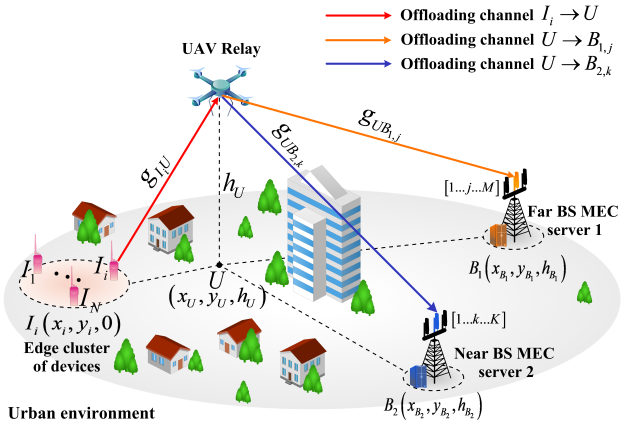

Fig. 1: System model for a UAV relay NOMA-MEC in IoT network.

Fig 1 illustrates a downlink NOMA-MEC system within an IoT network, where a UAV, denoted as U, is employed as an amplify-and-forward (AF) relay [15]. The U assists an ED cluster denoted by $I_i, i = 1...N$ in offloading tasks to two BS: far BS with M antennas denoted as $B_{f,j}, j = 1...M$, and near BS with K antennas denoted as $B_{n,k}, k = 1...K$. All nodes operate in half-duplex mode. Urban obstacles prevent direct connections between BSs and EDs. Utilizing a 3D Cartesian coordinate system, we denote $U\,(x_U, y_U, h_U)$, where $h_U > 0$; $B_f\,(x_{B_f}, y_{B_f}, h_{B_f})$; $B_n\,(x_{B_n}, y_{B_n}, h_{B_n})$; and $I_i\,(x_i, y_i, 0)$. The fading of the channel between the U and ground devices, follows a probabilistic LoS/NLoS model. Thus, mean path loss is considered as follows [16]:

$$\mathcal{L}_{ab} = \left[\mathcal{P}_{NLoS} + \frac{\mathcal{P}_{LoS} - \mathcal{P}_{NLoS}}{1 + \mathcal{B}e^{\left(-\frac{180}{\pi}\mathcal{A}\varphi_{ab} + \mathcal{AB}\right)}}\right] d_{ab}^{\sigma}, \quad (1)$$

where $ab \in (I_i U, UB_{f,j}, UB_{n,k})$, the elevation angle $\varphi_{ab} = \arcsin\left(\frac{h_U}{d_{ab}}\right)$ and the distance $d_{ab} = \sqrt{(x_b - x_a)^2 + (y_b - y_a)^2 + (h_b - h_a)^2}$; σ is the path-loss exponent; $\mathcal{A}$ and $\mathcal{B}$ are constant values that vary according to the surrounding environment; and $\mathcal{P}_\kappa = \mathcal{O}_\kappa(c/4\pi f_c)^{-1}$ is parameters depend on environment and carrier frequency, where $\kappa \in \{LoS, NLoS\}$, f_c is the carrier frequency, c is the speed of light, and $\mathcal{O}_\kappa$ is the excessive path losses of the LoS and NLoS propagation. Assuming I_i perform tasks of length L (bits) independently in groups [17]. B_f and B_n have MEC servers, and located at different distances from U. U forwards tasks from I_i, splitting them into subtask 1, denoted as $C_1^{off} = \beta L$ (bits) for B_f and denoted as $C_2^{off} = (1-\beta)L$ (bits) for B_n, where $\beta, (0 \le \beta \le 1)$ is the offloading ratio.

In practical wireless systems, achieving perfect channel state information (pCSI) is challenging due to channel estimation errors or feedback delays. Channel coefficients are modeled as $g_{ab} = \hat{g}_{ab} + e_{ab}$, where $\hat{g}_{ab}$ is the estimated channel coefficient and $e_{ab} \sim \mathcal{CN}(0, \mathcal{E}_{ab})$ denotes the channel estimation error with constant variance $\mathcal{E}_{ab}$ indicating the quality of channel estimation [18]. All channels are Nakagami-m fading channels with fading parameter m, and $\hat{g}_{ab}$ follows a Nakagami-m distribution. The study proposes a scheme to select best ED for task offloading to U and best antennas for receiving offloaded tasks, determining the channel power gain as $|\hat{g}_\psi|^2 = \arg\max\left(|\hat{g}_{ab}|^2\right)$, where $\psi \in (I_* U, UB_{f,*}, UB_{n,*})$. The work confines the fading parameter m to integer values across links, assuming uniformity in m values across all links analyzed. Thus, the probability density function (PDF) and cumulative distribution function (CDF) of the channel gain $|\hat{g}_\psi|^2$ are given as follows [11]:

$$f_{|\hat{g}_\psi|^2}(y) = \frac{\Xi y^{m-1}}{(m-1)!}\left(\frac{m}{\Omega_\psi}\right)^m \sum_{\tau=0}^{\Xi-1}\bigcup_{\tau}(-1)^\tau \times \Theta_{1,\tau}\Theta_{2,\tau} y^{\bar{\tau}} e^{-\frac{my(\tau+1)}{\Omega_\psi}}, \quad (2)$$

$$F_{|\hat{g}_\psi|^2}(y) = \sum_{\tau=0}^{\Xi}\bigcup_{\tau}(-1)^\tau \Theta_{1,\tau}\Theta_{2,\tau} y^{\bar{\tau}} e^{-\frac{\tau m y}{\Omega_\psi}}, \quad (3)$$

where $\Xi \in \{N, M, K\}$, $\Omega_\psi = \mathbf{E}\left\{|\hat{g}_\psi|^2\right\}$, $\bigcup_{\tau}\sum_{\tau_1=0}^{\tau}\sum_{\tau_2=0}^{\tau-\tau_1}\cdots\sum_{\tau_{(m-1)}=0}^{\tau-\tau_1-\ldots\tau_{(m-2)}}$, $\Theta_{1,\tau} = \binom{\Xi}{\tau}\binom{\tau}{\tau_1}\binom{\tau-\tau_1}{\tau_2}\cdots\binom{\tau-\tau_1-\ldots\tau_{(m-2)}}{\tau_{(m-1)}}$, $\Theta_{2,\tau} = \prod_{s=0}^{m-2}\left[\frac{1}{s!}\left(\frac{m}{\Omega_\psi}\right)^s\right]^{\tau_{(s+1)}}\left[\frac{1}{(m-1)!}\left(\frac{m}{\Omega_\psi}\right)^{m-1}\right]^{\tau-\tau_1-\ldots\tau_{(m-1)}}$ and $\bar{\tau} = (m-1)(\tau-\tau_1) - (m-2)\tau_2 - (m-3)\tau_3 \ldots - \tau_{(m-1)}$.

B. Communication protocol

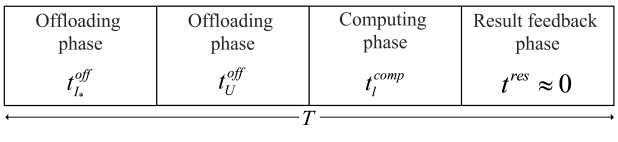

Fig. 2: Timing flowchart of our proposed model.

In this subsection, we present the proposed system's communication protocol, as shown in the time flowchart in Fig. 2.

- The first phase, $t_{I_*}^{off}$: I_* to offload L bits to U. Thus, the received signal at U is as $y_U =$

$\sqrt{\frac{P_{I_*}}{L_{I_*U}}}\left(\sqrt{\rho}x_f+\sqrt{(1-\rho)}x_n\right)g_{I_*U}+n_U$, where x_f and x_n are the offloaded signal to B_f and B_n, respectively; $g_{I_*U}=\hat{g}_{I_*U}+e_{I_*U}$; P_{I_*} is the transmit power of best ED; ρ is the power allocation ratio (PAC), $0.5<\rho\leq 1$; $n_U\sim\mathcal{CN}(0,N_0)$ is additive white Gaussian noise (AWGN).

- In the second phase, t_U^{off}: U performs the offloading of the received signal from I_* to $B_{l,*}, l\in(f,n)$ by using downlink NOMA technique [16], the signal received at B_l is given by $y_{B_{l,*}}=\frac{G}{\sqrt{L_{UB_{l,*}}}}y_U g_{UB_{l,*}}+n_{B_l}$, where P_U is the transmit power of U, G is the amplifying factor of the AF transition scheme, denoted by $G=\sqrt{\frac{P_U\mathcal{L}_{I_*U}}{P_{I_*}\left(|g_{I_*U}|^2+\mathcal{E}_{I_*U}\right)+\mathcal{L}_{I_*U}N_0}}$, and $n_{B_l}\sim\mathcal{CN}(0,N_l)$ is AWGN. Therefore, the received signal-to-interference-plus-noise ratios (SINRs) end-to-end at B_f and B_n for detecting x_f and x_n, respectively, are expressed as follows:

$$\gamma_1^{e2e}=\frac{\rho\gamma_I\gamma_U XY}{\gamma_U\left[(1-\rho)\gamma_I X+\mathcal{L}_{I_*U}\right]Y+\gamma_I\mathcal{L}_{UB_{f,*}}X+\vartheta_1}, \tag{4}$$

$$\gamma_2^{e2e}=\frac{(1-\rho)\gamma_I\gamma_U XZ}{\gamma_U\mathcal{L}_{I_*U}Z+\gamma_I\mathcal{L}_{UB_{n,*}}X+\vartheta_2}, \tag{5}$$

where $X=|g_{I_*U}|^2$, $Y=\left|g_{UB_{f,*}}\right|^2$, $Z=\left|g_{UB_{n,*}}\right|^2$, $\gamma_I=\frac{P_{I_*}}{N_0}$, $\gamma_U=\frac{P_U}{N_l}$, $\vartheta_1=\gamma_U\left[\mathcal{E}_{UB_{f,*}}\left(\gamma_I\mathcal{E}_{I_*U}+\mathcal{L}_{I_*U}\right)+\mathcal{L}_{UB_{f,*}}\mathcal{E}_{I_*U}\right]+\mathcal{L}_{I_*U}\mathcal{L}_{UB_{f,*}}$, and $\vartheta_2=\gamma_U\left[\mathcal{E}_{UB_{n,*}}\left(\gamma_I\mathcal{E}_{I_*U}+\mathcal{L}_{I_*U}\right)+\mathcal{L}_{UB_{n,*}}\mathcal{E}_{I_*U}\right]+\mathcal{L}_{I_*U}\mathcal{L}_{UB_{n,*}}$. Hence, the time offloading from I_* to $B_{l,*}$ is given by

$$t_l^{off}=\frac{C_l^{off}}{C_l^{x_l}}, \tag{6}$$

where $C_l^{x_l}=W\log_2\left(1+\gamma_l^{e2e}\right)$ is the instantaneous channel capacity of the $I_*\rightarrow B_{l,*}$ link, where W is the bandwidth.

- In the third phase, $t_{B_l}^{comp}$: B_l computes the offloaded tasks. The computation time is denoted as $t_l^{comp}=\frac{\varsigma C_l^{off}}{f_l^{MEC}}$, where ς is the number of CPU cycles required per input bit, and $f_{B_l}^{MEC}$ is the MEC operating frequency at B_l.
- In the fourth phase, t^{res}: B_l sends the computation results to I_* via U. The latency for returning results from B_l to I_* is neglected [11], as the returned data is significantly smaller than the offloaded data.

III. Performance Analysis

A. Successful computation probability (SCP)

In this subsection, we derive closed-form expressions for the SCP to evaluate the performance of the UAV relay-assisted NOMA-MEC system. SCP represents the probability that all tasks from the optimal edge device in the cluster are completed within the time period T. Thus, the SCP is calculated as follows [17]:

$$\Xi_l=\Pr\left\{t_l^{off}\leq T_l^{th}\right\}, \tag{7}$$

where $T_l^{th}=T-t_l^{comp}$.

Lemma 1: The closed-form expression for the SCP of the far BS for UAV relay-assisted NOMA-MEC under quasistatic Nakagami-m fading is given by:

$$\begin{aligned}\Xi_f=2\theta_1\sum_{j=1}^{M}\sum_{j_1=0}^{j}\sum_{i=0}^{N-1}\sum_{i_1=0}^{i}\sum_{t_1=0}^{m+\bar{i}-1}\sum_{t_2=0}^{\bar{j}}\theta_2\theta_3\theta_4\\ \times(\varphi_1)^{m+\bar{i}-1-t_1}(\varphi_2)^{\bar{j}}(\varphi_4)^{\bar{j}-t_2}e^{-\frac{mj\varphi_2}{\Omega_{B_f}}-\frac{m(i+1)\varphi_1}{\Omega_I}}\\ \times(\Delta_1)^{\frac{t_1+t_2-\bar{j}+1}{2}}\mathcal{K}_{t_1+t_2-\bar{j}+1}(\Delta_2),\end{aligned} \tag{8}$$

where $\theta_1=-\frac{NM!(N-1)!}{(m-1)!}\left(\frac{m}{\Omega_I}\right)^m$, $\theta_2=\frac{(-1)^j}{(M-j)!j_1!(j-j_1)!}\frac{(-1)^i}{(N-1-i)!i_1!(i-i_1)!}$, $\theta_3=\frac{(m+\bar{i}-1)!}{t_1!(m+\bar{i}-1-t_1)!}\frac{\bar{j}!}{t_2!(\bar{j}-t_2)!}$, $\theta_4=\left[\frac{1}{(m-1)!}\left(\frac{m}{\Omega B_f}\right)^{m-1}\right]^{j-j_1}\left[\frac{1}{(m-1)!}\left(\frac{m}{\Omega_I}\right)^{m-1}\right]^{i-i_1}$, $\varphi_1=\frac{\phi_1\mathcal{L}_{I_*U}}{\gamma_I[\rho-(1-\rho)\phi_1]}$, $\varphi_2=\frac{\phi_1\mathcal{L}_{UB_{f,*}}}{\gamma_U[\rho-(1-\rho)\phi_1]}$, $\varphi_3=\frac{\phi_1\vartheta_1}{\gamma_I\gamma_U[\rho-(1-\rho)\phi_1]}$, $\varphi_4=\frac{\varphi_2\varphi_1+\varphi_3}{\varphi_2}$, $\phi_1=2^{\frac{C_{IA_1}^{off}}{WT^{th}}}-1$, $\Delta_1=\frac{j(\varphi_2\varphi_1+\varphi_3)\Omega_I}{(i+1)\Omega_1}$, $\Delta_2=2m\sqrt{\frac{j(i+1)(\varphi_2\varphi_1+\varphi_3)}{\Omega_{B_f}\Omega_I}}$ and $\mathcal{K}_v(.)$ is Bessel functions [19].

Proof 1: See the section Proof of **Lemma 1**.

Lemma 2: The closed-form expression for the SCP of the near BS for UAV relay-assisted NOMA-MEC under quasistatic Nakagami-m fading is given by:

$$\begin{aligned}\Xi_n=2\lambda_1\sum_{j=1}^{K}\sum_{j_1=0}^{j}\sum_{i=0}^{N-1}\sum_{i_1=0}^{i}\sum_{t_1=0}^{m+\bar{i}-1}\sum_{t_2=0}^{\bar{j}}\lambda_2\theta_3\lambda_4\\ \times(\varphi_5)^{m+\bar{i}-1-t_1}(\varphi_6)^{\bar{j}}(\varphi_8)^{\bar{j}-t_2}e^{-\frac{mj\varphi_6}{\Omega_{B_n}}-\frac{m(i+1)\varphi_5}{\Omega_I}}\\ \times(\Delta_3)^{\frac{t_1+t_2-\bar{j}+1}{2}}\mathcal{K}_{t_1+t_2-\bar{j}+1}(\Delta_4),\end{aligned} \tag{9}$$

where $\lambda_1=-\frac{NK!(N-1)!}{(m-1)!}\left(\frac{m}{\Omega_I}\right)^m$; $\lambda_2=\frac{(-1)^j}{(K-j)!j_1!(j-j_1)!}\frac{(-1)^i}{(N-1-i)!i_1!(i-i_1)!}$, $\lambda_4=\left[\frac{1}{(m-1)!}\left(\frac{m}{\Omega B_n}\right)^{m-1}\right]^{j-j_1}\left[\frac{1}{(m-1)!}\left(\frac{m}{\Omega_I}\right)^{m-1}\right]^{i-i_1}$, $\varphi_5=\frac{\phi_2\mathcal{L}_{I_*U}}{(1-\rho)\gamma_I}$, $\varphi_6=\frac{\phi_2\mathcal{L}_{UB_{n,*}}}{(1-\rho)\gamma_U}$, $\varphi_7=\frac{\phi_2\vartheta_2}{(1-\rho)\gamma_I\gamma_U}$, $\varphi_8=\frac{\varphi_6\varphi_5+\varphi_7}{\varphi_6}$, $\phi_2=2^{\frac{C_2^{off}}{WT_2^{th}}}-1$, $\Delta_3=\frac{j(\varphi_5\varphi_6+\varphi_7)\Omega_I}{(i+1)\Omega_2}$, and $\Delta_4=2m\sqrt{\frac{j(i+1)(\varphi_5\varphi_6+\varphi_7)}{\Omega_{B_n}\Omega_I}}$.

Proof 2: The proof is similar to that of Lemma 1.

B. Optimization

To enhance offloading performance, we aim to optimize the computation performance of B_l by determining the optimal U deployment location (x_U^*,y_U^*,h_U^*). We formulate and solve

the SCP maximization problem using a GA-based algorithm [20].

SCP maximization problem:

$$\begin{aligned}
\text{(P1):}\ \underset{x_U, y_U, h_U}{\text{maximize}} \quad & S_l \\
\text{subject to} \quad & x_U^{\min} \le x_U \le x_U^{\max}, && \text{(10a)} \\
& y_U^{\min} \le y_U \le y_U^{\max}, && \text{(10b)} \\
& 0 \le h_U \le h_U^{\max}, && \text{(10c)}
\end{aligned}$$

where constraints (10a) and (10b) specify conditions for the UAV's ground location, while constraint (10c) addresses its altitude. To solve the constrained problem 10, we use the GA, known for its adaptability and ease of implementation, and it is detailed in **Algorithm 1**.

Algorithm 1 SCPMax-GA

Parameters $\mathcal{N}$, $\mathcal{I}$, S_l, γ, σ, β and constraint conditions

Generate the random solutions $\mathcal{X}_i(x_U^*, y_U^*, h_U^*)$

Evaluate the solutions with the fitness function $\mathcal{C}_i = 1 - S_l(\mathcal{X}_i)$

Loops until the termination

Parent selection-based roulette-wheel from the population

Uniformly crossover operation for new population generation with the probability of γ

Perform mutation on the new population with the rate of σ

Sort the top offsprings in the population and reject the others

Return: The greatest chromosome with the optimal (x_U^*, y_U^*, h_U^*) values.

IV. Numerical Result

In this section presents numerical results to validate the SCP analytical expression for UAV-assisted NOMA-MEC in IoT networks, using the system parameters [11], such as average transmit signal-to-noise ratio (SNR) $\gamma_U = [0, 20]$ (dB), $\gamma_I = [0, 20]$ (dB), $(x_I, y_I) = (-100, 0)$, $(x_{B_f}, y_{B_f}, h_{B_f}) = (100, 100, 5)$, $(x_{B_n}, y_{B_n}, h_{B_n}) = (100, -50, 5)$, $T = 0.5$ (s), $\rho = 0.75$, $\beta = 0.6$, $\mathcal{A} = 0.1581$, $\mathcal{B} = 9.6177$, $\mathcal{O}_{LoS} = 1$, $\mathcal{O}_{NLoS} = 20$, $c = 3.10^8$ (m/s), $W = 10^5$ (Hz), $f_c = 10^4$, $f_U^{MEC} = 10^8$, $\varsigma = 5$, $\mathcal{I} = 10^2$, and $\mathcal{N} = 50$.

Fig. 3 shows the effect of average transmission SNR of ED on SCPs with varying offload task lengths L. The first observation is the match between simulation and analysis results, confirming the accuracy of our model. The second observation is that as the ED's transmission capacity increases, offload performance improves. However, increasing the computational task length reduces SCP. This is because longer tasks require more offload time, increasing transition and processing times, thus decreasing SCP performance.

Fig. 4 demonstrates the effect of average transmission SNR of the UAV on SCPs with different channel estimation error values $\mathcal{E}$. Similar to Fig. 3, increasing the UAV's transmission

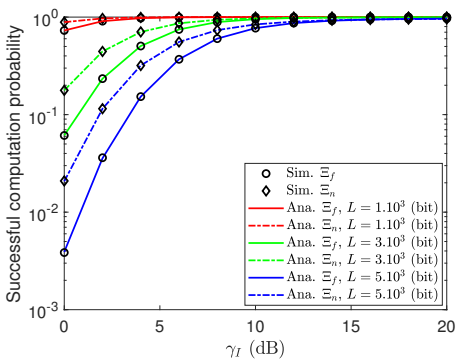

Fig. 3: Impact of γ_I on SCPs of the far BS and near BS with various offload task lengths L.

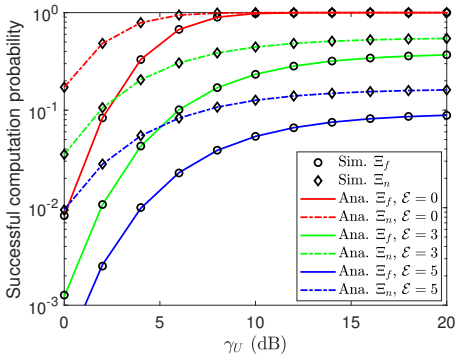

Fig. 4: Impact of γ_U on SCPs of the far BS and near BS with various channel estimation errors $\mathcal{E}$.

power, SCP increases, as the UAV has more energy to relay information to the BSs. Channel estimation errors significantly impact offloading performance. When $\mathcal{E} = 0$ (pCSI), the offloading performance is optimal, although this scenario is unlikely in real wireless environments. Higher values of $\mathcal{E} = 3$ and $\mathcal{E} = 5$ (indicating imperfect channel state information (iCSI)) degrade system performance, as noisy channel information makes signal decoding difficult, reducing SCP.

Fig. 5 illustrates the impact of UAV altitude (h_U) on SCPs with varying numbers of EDs (Fig. 5a) and antennas (Fig. 5b). SCP is maximized at an optimal altitude due to the balance between LoS and NLoS conditions. At low altitudes, urban obstacles hinder communication, reducing offloading efficiency. As altitude increases, LoS improves while NLoS decreases, but excessive height causes high transmission loss. Thus, SCP peaks at a optimal altitude (h_U^*). Additionally, increasing the number of EDs and antennas enhances performance by providing more optimal communication options.

Besides altitude, the UAV's location is crucial for optimal communication with ED and BS. Fig. 6 presents a 3D visualization of SCP values influenced by x_U and y_U. Fig. 6a and 6b show the optimal UAV positions for far BS and near BS, respectively. There are optimal coordinates, x_U^* and y_U^*, that maximize system performance, as the UAV seeks the best

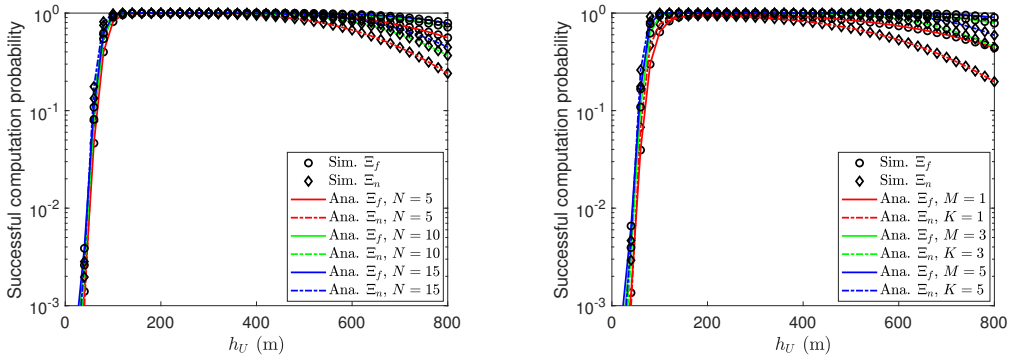

(a) SCPs with various N

(b) SCPs with various M and K

Fig. 5: Impact of h_U on SCPs of the far BS and near BS.

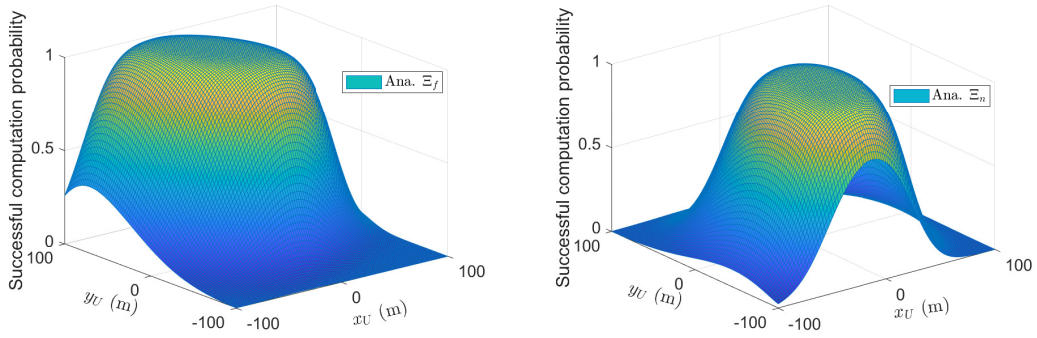

(a) B_f with various (x_U, y_U)

(b) B_n with various (x_U, y_U)

Fig. 6: Impact of location (x_U, y_U) on SCP of the far BS and near BS

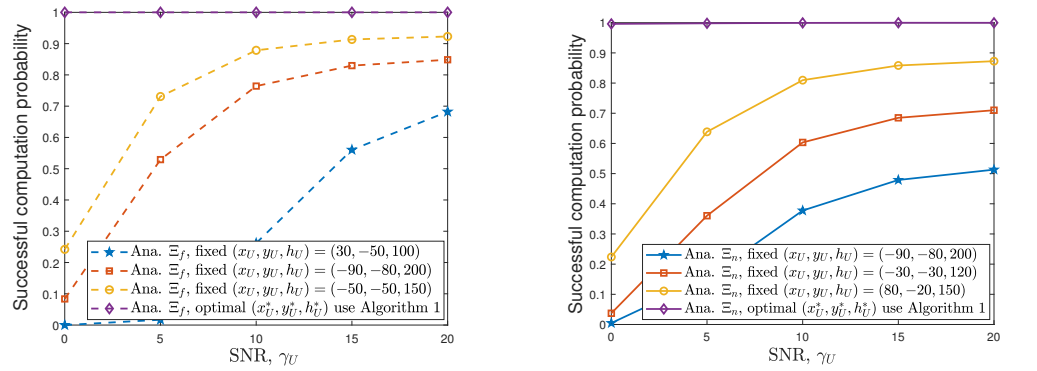

(a) Compare the deployment position of the U with B_f

(b) Compare the deployment position of the U with B_n

Fig. 7: Impact of (x_U^*, y_U^*, h_U^*) on SCP of the far BS and near BS

TABLE I: Algorithm results.

	Far BS			**Near BS**		
γ_U (dB)	x_U^* (m)	y_U^* (m)	h_U^* (m)	x_U^* (m)	y_U^* (m)	h_U^* (m)
0	6.075	50.639	206.963	6.416	-22.170	246.212
5	2.421	50.114	262.401	1.453	-25.370	182.035
10	0.555	49.110	212.158	-0.362	-24.896	182.037
15	-0.615	49.725	197.660	-1.601	-25.150	206.337
25	2.717	39.839	216.742	-1.265	-24.381	184.163

position to communicate with both ED and BS. This highlights a key advantage of using UAV.

Fig. 7 shows the impact of the UAV's optimal position and height, (x_U^*, y_U^*, h_U^*), on the SCP of far BS (Fig. 7a) and near BS (Fig. 7b). Using optimal values derived from solving the optimization problem (Table I), we compare SCP at optimal values with SCP at fixed values. The results indicate that applying the SCPMax-GA algorithm for optimal

values significantly improves offload performance compared to manually setting the UAV's position.

V. Conclusion

This paper investigates the offloading performance of a UAV relay-assisted NOMA-MEC system in IoT networks using Nakagami-m fading channels. To improve offloading performance, a four-phase system operating protocol based on ED and antenna selection via NOMA approaches is presented. Closed-form equations for the SCPs of far and near BS are obtained. In addition, a GA-based algorithm is used to optimize the UAV's location and height in order to enhance SCP. The numerical findings support the system's offloading performance.

Proof of Lemma 1

By substituting (2), (3), (4), (6) into (7), we can rewrite the Ξ_1 as:

$$S_1 = \Pr\left\{X \geq \varphi_1, Y \geq \frac{\varphi_2 X + \varphi_3}{X - \varphi_1}\right\} = \int_{\varphi_1}^{\infty} \left[1 - F_Y\left(\frac{\varphi_2 X + \varphi_3}{X - \varphi_1}\right)\right] f_X(X)\, dX. \quad (11)$$

where $\varphi_1 = \frac{\phi_1 \mathcal{L}_{I_* U}}{\gamma_I[\rho-(1-\rho)\phi_1]}$, $\varphi_2 = \frac{\phi_1 \mathcal{L}_{UB_{f,*}}}{\gamma_U[\rho-(1-\rho)\phi_1]}$, $\varphi_3 = \frac{\phi_1 \vartheta_1}{\gamma_I \gamma_U[\rho-(1-\rho)\phi_1]}$. First, we replace PDF in (2) and CDF in (3). After a few mathematical transformations and applying the Bessel function [19], we obtain the closed form expression. This concludes our proof.

References

[1] J. Liu, A. Zhou, C. Liu, T. Zhang, L. Qi, S. Wang, and R. Buyya, "Reliability-enhanced task offloading in mobile edge computing environments," *IEEE Internet of Things J.*, vol. 9, no. 13, pp. 10 382–10 396, Jul. 2022.

[2] Z. Ding, D. Xu, R. Schober, and H. V. Poor, "Hybrid noma offloading in multi-user mec networks," *IEEE Trans. Wireless Commun.*, vol. 21, no. 7, pp. 5377–5391, Jul. 2022.

[3] C. Shang, Y. Sun, H. Luo, and M. Guizani, "Computation offloading and resource allocation in noma–mec: A deep reinforcement learning approach," *IEEE Internet of Things J.*, vol. 10, no. 17, pp. 15 464–15 476, Sep. 2023.

[4] B. Bahrami, M. R. Khayyambashi, and S. Mirjalili, "Edge server placement problem in multi-access edge computing environment: models, techniques, and applications," *Cluster Comput.*, vol. 26, no. 5, pp. 3237–3262, Oct 2023.

[5] M. Ghous, A. K. Hassan, Z. H. Abbas, G. Abbas, A. Hussien, and T. Baker, "Cooperative power-domain noma systems: An overview," *Sensors*, vol. 22, no. 24, Dec. 2022.

[6] L. Lin, W. Zhou, and Z. Zhao, "Analytical modeling of noma-based mobile edge computing systems with randomly located users," *IEEE Commun. Lett.*, vol. 24, no. 12, pp. 2965–2968, Dec. 2020.

[7] X. Dong, X. Li, X. Yue, and W. Xiang, "Performance analysis of cooperative noma based intelligent mobile edge computing system," *China Commun.*, vol. 17, no. 8, pp. 45–57, Aug. 2020.

[8] H. Jiang, Y. Wang, X. Yue, and X. Li, "Performance analysis of noma-based mobile edge computing with imperfect csi," *EURASIP J. Wireless Commun. Networking*, vol. 2020, no. 1, p. 138, Jul 2020.

[9] M. Mehrabi, D. You, V. Latzko, H. Salah, M. Reisslein, and F. H. P. Fitzek, "Device-enhanced mec: Multi-access edge computing (mec) aided by end device computation and caching: A survey," *IEEE Access*, vol. 7, pp. 166 079–166 108, Nov. 2019.

[10] Y. Zeng, R. Zhang, and T. J. Lim, "Wireless communications with unmanned aerial vehicles: opportunities and challenges," *IEEE Commun. Mag.*, vol. 54, no. 5, pp. 36–42, May 2016.

[11] A.-N. Nguyen, D.-B. Ha, V. N. Vo, V.-T. Truong, D.-T. Do, and C. So-In, "Performance analysis and optimization for iot mobile edge computing networks with RF energy harvesting and UAV relaying," *IEEE Access*, vol. 10, pp. 21 526–21 540, Feb. 2022.

[12] A. Umar, S. A. Hassan, H. Jung, S. Garg, M. S. Hossain, and M. Guizani, "Computation offloading in noma-mec-enabled aerial-vehicular networks exploiting mmwave capabilities," *Comput. Networks*, vol. 246, p. 110335, Jun. 2024.

[13] G.-H. Nguyen, A.-N. Nguyen, H.-H. Le, and T.-D. Do, "Energy harvesting and computation offloading for uav-assisted mec with noma in iot network," in *Communication and Intelligent Systems*, Singapore, 2024, pp. 381–392.

[14] X. Meng, C. Zhan, R. Huang, and J. Liao, "Computation throughput maximization for uav-enabled mec via uplink noma," in *IEEE Global Commun. Conf.*, Feb. 2023, pp. 6922–6927.

[15] A.-N. Nguyen, V. N. Vo, C. So-In, and D.-B. Ha, "System performance analysis for an energy harvesting iot system using a DF/AF UAV-enabled relay with downlink NOMA under nakagami-m fading," *Sensors*, vol. 21, no. 1, Jan. 2021.

[16] A.-N. Nguyen and N.-A. Bui, "Performance analysis of iot mobile edge computing networks using a df/af uav-enabled relay with downlink noma," in *2023 IEEE Symposium on Industrial Electronics & Applications (ISIEA)*, Aug. 2023, pp. 1–6.

[17] A.-N. Nguyen, T.-D. Do, G.-H. Nguyen, and H.-H. Le, "Uav relay-assisted noma mec in iot networks: Offloading performance and optimization," in *Communication and Intelligent Systems*, Singapore, 2024, pp. 393–408.

[18] A.-N. Nguyen, D.-B. Ha, T. V. Truong, V. N. Vo, S. Sanguanpong, and C. So-In, "Secrecy performance analysis and optimization for uav-relay-enabled wpt and cooperative noma mec in iot networks," *IEEE Access*, vol. 11, pp. 127 800–127 816, Nov. 2023.

[19] I. Gradshteyn and I. Ryzhik, *Table of Integrals, Series, and Products*, A. Jeffrey and D. Zwillinger, Eds. USA: Academic Press, 2014.

[20] X. Wen, Y. Ruan, Y. Li, H. Xia, R. Zhang, C. Wang, W. Liu, and X. Jiang, "Improved genetic algorithm based 3-d deployment of uavs," *J. Commun. Netw.*, vol. 24, no. 2, pp. 223–231, Apr. 2022.